Egyptian Journal of Chemistry

http://ejchem.journals.ekb.eg/

Thermal Degradation, Flame Retardancy and Mechanical Characterization of Modified WPP Composites by Microencapsulation Technique

A. A. Younis[1]* and A. A. El-Wakil[2]

*[1]*Fire and Explosion Protection Lab (FEP), National Institute of Standards, Tersa St, El-Matbaa, Haram, P. O. Box: 136, Code No. 12211 Giza, Egypt.*
[2]Polymer Metrology and Technology Laboratory, National Institute of Standards, Tersa St, El-Matbaa, Haram, P. O. Box: 136, Code No. 12211 Giza, Egypt.

Abstract

Encapsulation/coating of nanoparticles is a significant test return to the minuscule size and high surface energy with surface space of the nanoparticles. This manuscript, using waste chicken eggshell (WCES) particles as a core material and natural rubber-graft-acrylamide (NR-g-AAm) as the wall material or shell. Fourier Transform Infrared (FTIR) Spectroscopy and Scanning Electron Microscopy (SEM) were used to determine the main structure and surface analysis of encapsulated waste chicken eggshell (ENWCES) and novel composites. Mechanical and Dynamic Mechanical Analysis were tested. Thermal Analysis and flame retardant were applied to the specimens using thermal gravimetric analysis, Flame Chamber, and limiting oxygen index (LOI) according to standards. It has been established that microencapsulation enhanced the mechanical properties of WPP composites. This technique recorded the highest thermal stability and ash residue percentages. These enhancements still working on stopping ignition, whereas, these new compositions protect ignition up to 26%, which can be classified as a flame retardant.

Keywords: WPP, WCES, ENWCES, Fire resistant (Flame chamber, Oxygen index), Mechanical properties

;

Introduction

Polypropylene (PP) is one of the most consumed thermoplastics in the world. It is also representing the most polymeric waste that causes serious environmental problems. Therefore, the production of alternatives for waste polypropylene (WPP) recycling is important to produce new products of economic advantages. The incorporation of waste of bio fillers into WPP to produce biocomposites to enhance the properties of the WPP matrix and reduce environmental pollution has been reported as successful studies. WPP biocomposites are employed in a variety of sectors, including automobile synthesis, and construction [1]. Bio-composites fillers take attention from the researchers due to safety requirements achievement. Waste chicken eggshell (WCES) was employed as a bio filler to improve the mechanical and ignition properties of polypropylene (PP), The organic matter of WCES contains sialic acid, glycine, and alanine [2]. The WCES has been listed worldwide as one of the worst creators of environmental problems [3]. The WCES powder has also been used as a reinforcing filler in elastomers such as natural rubber (NR), acrylonitrile butadiene rubber (NBR), styrene-butadiene rubber (SBR), and epoxidized natural rubber (ENR) [4, 5]. The performance of WCES as a reinforcing agent in polymer composites depends on its compatibility with polymer matrix. As such, the surface of the WCES particles is usually modified to promote polymer–filler interactions. Additionally, surface functionalization using organic materials, may lower the surface energy value of the WCES phase and reduce the possibility of

*Corresponding author e-mail: dr_ahmedabdee@yahoo.com; ((A. A. Younis)).
Receive Date: 19 November 2021, **Revise Date:** 11 December 2021, **Accept Date:** 22 December 2021
DOI: 10.21608/EJCHEM.2021.106853.4903

agglomeration of the particles [6]. The tensile strength and thermal stability of high density polyethylene (HDPE)/WCES powder composites were improved with the modification of WCES by (3-Mercaptopropyl) trimethoxysilane as coupling agent due to the interaction and adhesion between HDPE and modified WCES were enhanced [7].

In previous works, WCES powder has been treated with stearic acid, isophthalic acid, and pimelic acid (PA) to improve the mechanical properties of polypropylene composites. 40 wt% of treated WCES by stearic acid improved the young's modulus of PP composite, whereas the crystallinity of PP composites containing WCES powder remained almost unchanged [8]. The elastic modulus of PP composites containing WCES treated with isophthalic acid improved by 18 % compared to composites containing WCES [9]. PA promoted the dispersion state of WCES in the PP matrix by decreasing the interfacial tension. Also, the modified WCES by PA caused a slight deterioration of both tensile and flexural strength of PP composite. The impact strength of the PP composite containing the modified WCES by PA enhanced compared to that of neat PP composite [10].

Microencapsulation is a procedure since liquid or solid could be encapsulated by a film-forming material to shape little particles. It is an important technique used to keep on the functional processes. The role of microencapsulation is to give the material new functions or enhancing its properties. The material enclosed is called core material and the cover material is called wall material or shell [11, 12]. Microencapsulation has numerous spaces of use, such as; flame retardants [13], cosmetics, dyes printing [14], and wood-plastic composites [15]. Microencapsulated ammonium polyphosphate propylene [16], and styrene-ethylene-butylene-styrene [17] have been used to enhance the ignition characteristics of materials. The fire is depending on the presence of four factors, oxygen, heat, fuel, interchemical reaction as found in fire tetrahedron [18]. Ignition is stopped by the absence of at least one of the four ignition factors before actual ignition occurs [19]. Calcium carbonate ($CaCO_3$) was used to synthesis a new flame retardant coating to protect bagasse paper from the ignition [20].

Disposal of polymer and eggshell wastes in landfills is a serious challenge in developing countries. Polymer and eggshell wastes are permanent contaminants to the local environment, including soil and water [21]. Therefore, this article aims to produce and characterize new composites of waste polypropylene and encapsulated renewable waste chicken eggshells. The WCES is coated or encapsulated by natural rubber-g-acrylamide (NR-g-AAm) to improve reinforcing characteristics. The mechanical, and dynamic mechanical were investigated thermal, and ignition properties of new WPP composites.

Experimental

Materials

Natural rubber (type SIR 20), were supplied by Engineering and transportation company, Egypt. Acrylamide was provided by the Egyptian British Co., Egypt. Mohr's salt, Benzoyl peroxide was obtained from Research LAB Fine Chem. Industries and Loba Chemie Pvt. Ltd, Mumbai, India. soap packs of waste polypropylene (WPP) were collected, washed, dried, cut into small pieces (1 cm× 1 cm).

Synthesis of NR-g-AAm

Reactions were carried out in a round bottom flask equipped with a nitrogen inlet, thermometer, and reflux condenser. The reaction flask contains 10 gm of NR in toluene was heated and stirring to dissolve the NR. When the dissolution was complete, one gm of acrylamide (AAm), 0.3 gm of mohr's salt, and 1.0 % of benzoyl peroxide as free radical initiator were added to the reaction mixture. The time of addition of the reaction component was recorded as the starting time of the reaction. After reaching the desired time, the reaction was stopped and the grafting product was precipitated in ethanol, repeatedly washed with ethanol to remove unreacted AAm, and finally, it was filtered and dried at 50 °C to a constant weight. To remove all the unreacted AAm, the precipitated polymer was dissolved in toluene and refluxed for 4 h and it was then again precipitated in ethanol, washed, and finally dried. The Grafting Degree (GD) can be calculated from equation 1 [22].

$$\text{Grafting Degree} = [Wg/WNR] \times 100 \quad (1)$$

where WNR is the weight of NR and Wg is the weight of the graft yield. The degree of grafting was calculated and is reported in Table 1

Table 1: Degree of grafting of NR-g-AAm

Grafting product	Degree of grafting (%)
NR-g-AAm	15.5

Encapsulation of WCES by NR-g-AAm

The procedure employed for the encapsulation of WCES was as follows. 1.0 gm NR-g-AAm, and 100 mL toluene were transferred into a 500 mL three-necked flask. 100 gm WCES was added to the above solution. The mixture of WCES and NR-g-AAm was stirred vigorously for 60 min using a mechanical stirrer at 100 ºC in order to ensure that mixture components could react completely. The encapsulated WCES (ENWCES) was dried for 120 min in an oven at 100 ºC, resulting in a 1 % modified WCES [23].

WPP/WCES and WPP/ ENWCES Composites preparations

WPP was mixed with WCES powders and ENWCES (0, 10, 20, and 30 wt. percent) at 190 ºC for 10 min at 80 rpm in a closed Brabender Plasti Corder Lab Station (Brabender, USA). Finally, the WPP composites were molded using a hot press at 190 ºC for 30 s followed by a cold press machine. Before the tests, test specimens were conditioned for at least 40 h at 23 °C and 50% relative humidity [24]. Table 2 contains the definitions of the WPP

FTIR spectroscopy

The FTIR spectra of the WPP composites were measured with a Nicolet 380 Spectrometer Instrument (USA) with an average of 32 scans and a spectral resolution of 4 cm^{-1} in the wavenumber range of 500 to 4000 cm^{-1} [25].

Scanning electron microscopy (SEM)

The surface morphology of the composites was studied using a Scanning Electron Microscopy instrument, Quanta FEG-250, FEI Company (USA), with a 20 kV acceleration voltage. It was carried out after a thin layer of gold/palladium alloy (less than 2 nm) was applied to the specimen's surface using a Leica EM ACE200 coating equipment [2].

Mechanical properties

WPP composites were put through a tensile test in accordance with ASTM D 638 [26] using a Zwick Tensile Testing machine (Model Z010, Germany) with a crosshead speed of 50 mm/min on a type V specimen. Flexural test for WPP composites performed according to ASTM D 790 [27] at a crosshead speed of 3 mm/min using the same testing machine as above. Three specimens were tested for each type of WPP composite, and the average values were reported.

Dynamic mechanical analysis (DMA)

It's been used to examine the viscoelastic behaviour of polymers for a long time. The DMA device (DMA Q800: supplied by TA Instrument, USA) was calibrated according to the manufacturer's recommended procedures. In the tension mode of deformation, the storage modulus and loss factor (tan δ) were measured. In presence of liquid nitrogen, these properties were measured at 1 Hz, in the temperature range between -75 ºC and 75 ºC with a heating rate of 5 ºC/min [28].

Table 2: Formulation of WPP Composites

Codes / Composites	MOS1	MOS2	MOS3	MOS4	MOS5	MOS6	MOS7
WPP /(phr)	100	100	100	100	100	100	100
WCES /(phr)	-----	10	20	30	---	----	----
ENWCES /(phr)	-----	------	------	------	10	20	30

While; phr: Part per hundred part, MOS1: This composite is made up of 100 phr waste polypropylene alone, MOS2: This composite is made up of 100 phr waste polypropylene and 10 phr waste chicken eggshell, MOS3: This composite is made up of 100 phr waste polypropylene and 20 phr waste chicken eggshell, MOS4: This composite is made up of 100 phr waste polypropylene and 30 phr waste chicken eggshell, MOS5: This composite is made up of 100 phr waste polypropylene and 10 phr of encapsulated waste chicken eggshell, MOS6: This composite is made up of 100 phr waste polypropylene and 20 phr of encapsulated waste chicken eggshell, and MOS7: This composite is made up of 100 phr waste polypropylene and 30 phr of encapsulated waste chicken eggshell.

Thermal and ignition technique

Thermal shrinkage

The thermal shrinkage measurements were done at ages of 1 hr of drying at Binder oven, IP20 (USA) country. The dimension of the specimens was 20 mm x 20 mm x 2 mm. Firstly, the specimen weighted before testing (W1) then after heating at 150 ºC for 1 hr (W2). Equation 2 was used to compute the thermal shrinkage [29]:

Thermal shrinkage (%) = [1- (W2/W1)] x 100 (2)

Thermal analysis technique

The stages of decay, and percentage of weight loss, and ash residue of WPP composites were measured. This test was carried out in accordance with ISO 11358 [30] using a Shimadzu TGA-50 Instrument (Japan) at a temperature of 35 and 700 ºC, with sample weight of 10 mg, a flow rate of 30 ml/min, and a heating rate of 10 ºC/min. These measures were performed under nitrogen gas.

Limiting oxygen index (LOI)

These tests were performed according to different standards. Firstly, ISO 4589 [31, 32] standard was used to determine the minimum oxygen percentage keep ignition of the specimen. This test was achieved in Oxygen Index Tester (Rheometric Instrument, Japan) using samples in dimensions 125 mm × 10 mm × 4 mm with a length of 25 mm of propane gas as a flame source. The specimen was clamped vertically in a holder (U shape), exposed to flame for 30 s from the free edge, then removed the flame source and ignition properties of the test specimen was studied up to 180 s. The LOI percentage was considered after an average of three replicates was tested.

Flame chamber (UL-94)

Secondly, the burning rate (BR) was calculated according to ASTM D 635 [33]. The specimens were cut in dimension 125 mm × 10 mm × 4 mm, hold vertically, and exposed to methane flame source for 15 s then removed. The ignition time and length of ignited area after first line were measured and burning rate (BR) was calculated from this equation 3 [34]:

$$BR = 60 \times L/t \quad (3)$$

where L is the burned length (millimeters) and t is the time of burning after first line (minutes).

Results and Discussion

Characterization of NR-g-AAm, WCES, and ENWCES

The FTIR data of the NR, AAm, and NR-g-AAm is represented in figure. 1-A. The FTIR spectrum of the AAm shows the existence of the N-H symmetric and asymmetric stretch indicated by the absorption peaks at 3171 and 3343 cm^{-1}. The absorption bands at 1664 cm^{-1} (C=O) and 1605 cm^{-1} (C=C) are characteristics of the acrylamide unit [35]. FTIR spectrum of NR shows the characteristic peak of the (-C=C-) group at 1666 cm^{-1}. FTIR spectrum of NR-g-AAm shows the disappearance of the absorption peaks of (-C=C-) groups in NR and AAm and new absorption peaks at 1703 and 3396 cm^{-1} attributed to (C=O) stretch and N-H, respectively. This confirms the graft copolymerization on AAm onto the NR [36]. The synthesis of NR-g-AAm has graphically presented in the schematic in figure. 1-C.

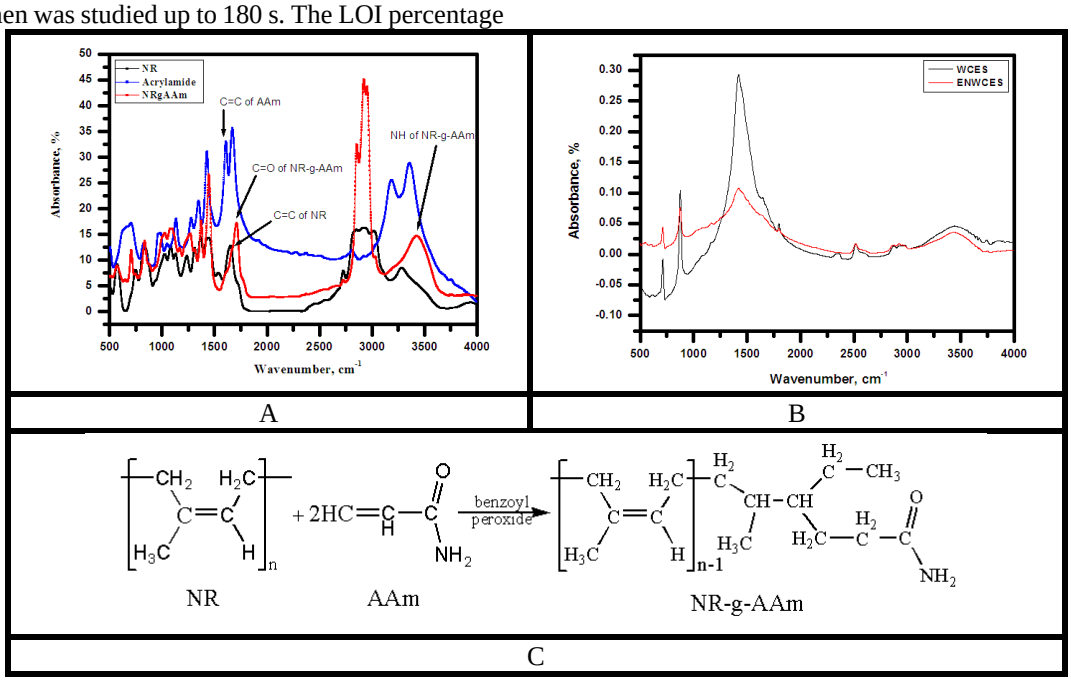

Figure 1: FTIR spectra of A) NR, Acrylamide and NR-g-AAm; B) WCES, and ENWCES powders, while C) Schematic of synthesis of NR-g-AAm.

The chemical structure before and after modification of WCES particles was investigated by FTIR spectra as depicted in figure 1-B. It can be seen that WCES represent characteristic peaks at 1412, 871, and 707 cm^{-1}, representing the asymmetric stretch, out-of-plane bend, and in-plane bending vibrations of CO_3^{2-} ion, respectively. The absorption bands situated at 1795, 2344, 2504, 2851, and 2983 cm^{-1} were identified as organic matter and a broad absorption band at 3425 cm^{-1} was due to the stretching vibration of structural H_2O [37] By comparing between FTIR spectra of WCES, NR-g-AAm, and ENWCES is evident that the asymmetric stretch, out-of-plane bend, and in-plane bending vibrations of CO_3^{2-} ion and the stretching vibration of structural H_2O decrease in intensity to a great extent, indicating organic matter and $CaCO_3$ of WCES particles react with NR-g-AAm [38].

Morphology of the WCES and ENWCES powders

Figure 2 (A and B) show the SEM photographs of WCES and ENWCES powders. Figure 2-A elucidates the WCES powder has a strong tendency of agglomeration. This was due to the small particle size and high surface energy of waste eggshell powder. Figure 2-B illustrates the ENWCES powder becomes less agglomerate compared to WCES powder because the nature of the WCES powder surface changed and the growth of film of NR-g-AAm on the surface of the WCES powder [39]. The particle size of WCES and ENCAP WCES is estimated to be about 356.84 nm and 2.36 µm.

Morphology of the WPP/WCES and WPP/ ENWCES composites

Figure 2 displays the scanning electron microscopy morphology of WPP (MOS1), WPP/WCES (MOS2, MOS4), and WPP/ENWCES (MOS5, MOS7). The morphology of the WPP/WCES composites containing 10 and 30 phr of WCES is shown in figure 2 (MOS2 and MOS4). They illustrate these composites have some aggregation of WCES and micro-voids surrounded by some of them. These indicate that the interfacial adhesion was weak between the WPP matrix and WCES [40]. The scan of (MOS5 and MOS7) show the SEM micrographs of the WPP/ENWCES composites containing 10 and 30 phr of ENWCES, respectively. When compared with (MOS1, MOS2, and MOS4), WPP/ENWCES composites appeared to yield improved interfacial adhesion between WPP and ENWCES filler, which resulted in an excellent improvement in the dispersion of WCES and the reaction between the WPP and ENWCES. This indicates that the encapsulation process of WCES promotes adhesion between the WCES and WPP matrix [41].

X-Ray Diffraction Analysis

Figure 3 shows the patterns of XRD diffraction of the prepared composites in the 2θ range of 4-70°. The neat WPP composite diffraction peaks appeared at 2θ, 14.06°, 16.86°, 18.51°, 21.21°, and 21.8° for the lattice planes 110, 040, 130, 111, and 131, respectively [42]. WPP/WCES, and WPP/ENWCES composites with 10 and 30 phr of WCES and ENWCES displayed diffraction peaks at 2θ, 23.10°, 29.50°, 36.05°, 39.52°, 43.25°, 47.50°, 48.58°, 57.54° for the lattice planes 012, 104, 110, 113, 202, 018, 116, and 122 respectively plus the diffraction peaks of WPP composite [43].

By comparison of XRD diffraction patterns of neat WPP, WPP/WCES, and WPP/ENWCES composites, the intensity of XRD peaks of WPP, WCES decrease in XRD patterns of WPP/ENWCES composites. It may return to the reactions between WPP, WCES, and ENWCES. These findings are in line with those found in a previous study [44], where it was discovered that the treated acrylamide had a direct influence on lowering the XRD peak intensity. The decrease in intensity of crystalline planes after treatment with acrylamide may be due to the disturbed regular pattern of the atoms.

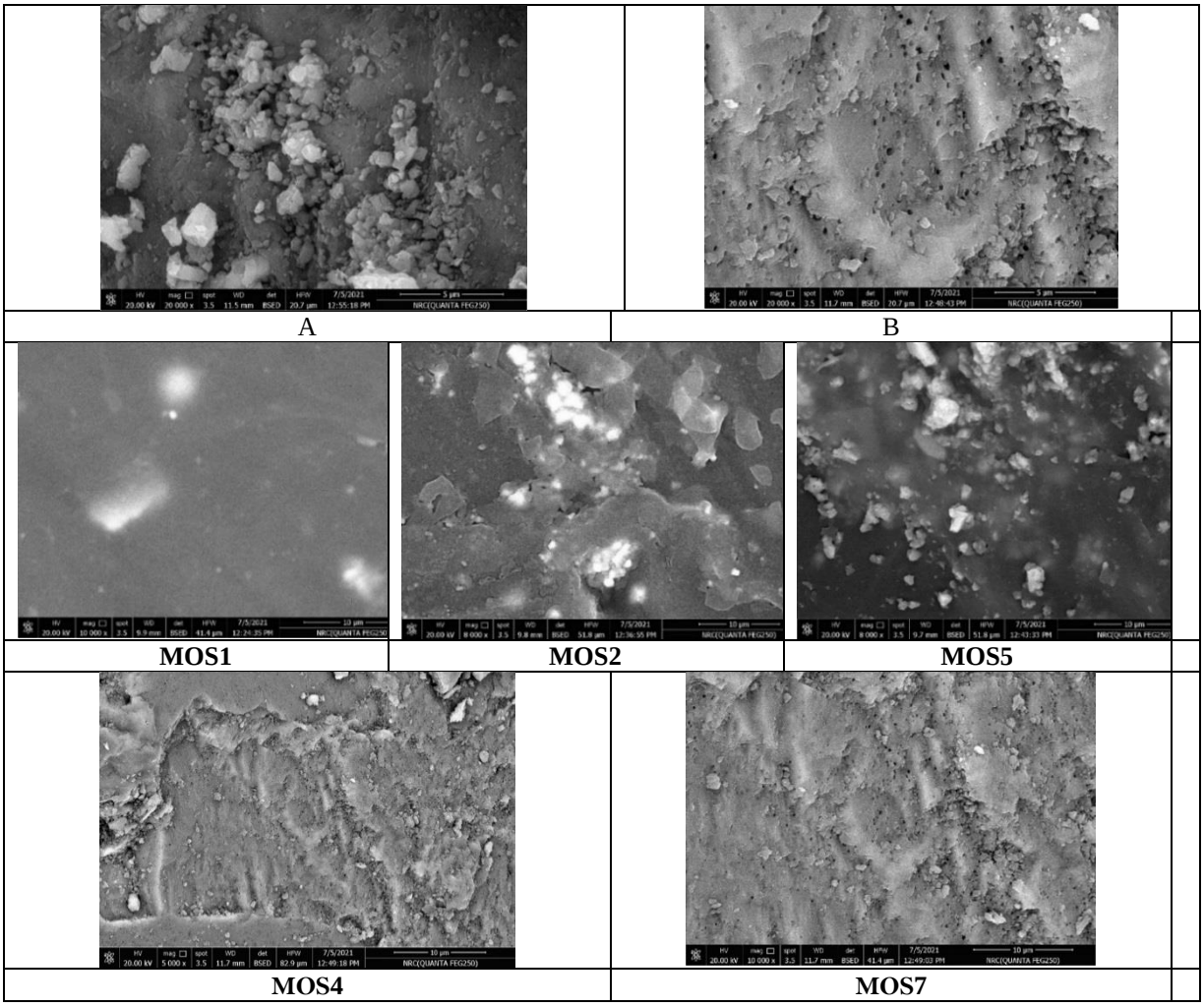

Figure 2: SEM photographs of (A) WCES, and (B) ENWCES powders, and the SEM photographs of MOS1-7 composites

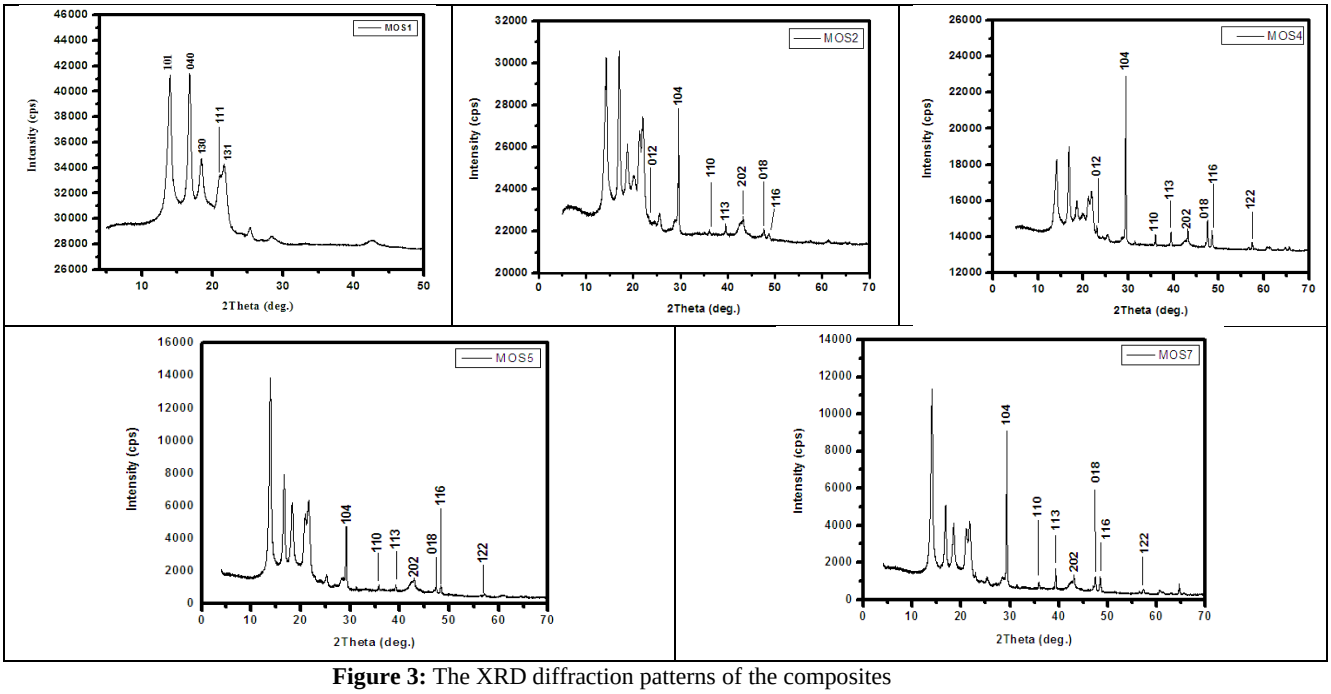

Figure 3: The XRD diffraction patterns of the composites

Mechanical properties

WCES and ENWCES were fused into the WPP matrix to accomplish better support of the matrix, so it is beneficial to investigate the impact of WCES and ENWCES content on the mechanical properties of WPP composites. It was noticed from figure 4, an increment in tensile strength, and flexural strength of WPP composites with the addition of 10 phr of WCES, yet the joining of the large content of WCES (20 and 30 phr) lead to abatement in these properties. When the WCES material is increased to 30 phr, the elongation at maximum is reduced and the flexural modulus of WPP composites is increased. This figure shows the incorporation of ENWCES (10, 20, and 30 phr) upgrades the tensile strength, elongation at maximum, flexural strength, and flexural modulus of WPP/ENWCES composites contrasted with neat WPP and WPP/WCES composites. While, 10 phr of ENWCES enhance the tensile strength, elongation at maximum, and flexural strength of WPP composites by 19.20 %, 42.70 %, and 41.85 %, respectively, contrasted with WPP composite.

With the expansion of the ENWCES stacking to 20 phr the tensile strength, elongation at maximum, and flexural strength of the WPP composites diminishes, and these properties marginally decline with the constant increment of the ENWCES loading to 30 phr. Nonetheless, the WPP/ENWCES composite that contains 30 % of the ENWCES actually accomplished better tensile strength, elongation at maximum, and flexural strength by 8.87 %, 5.70 %, and 8.80% than that of the WPP composite.

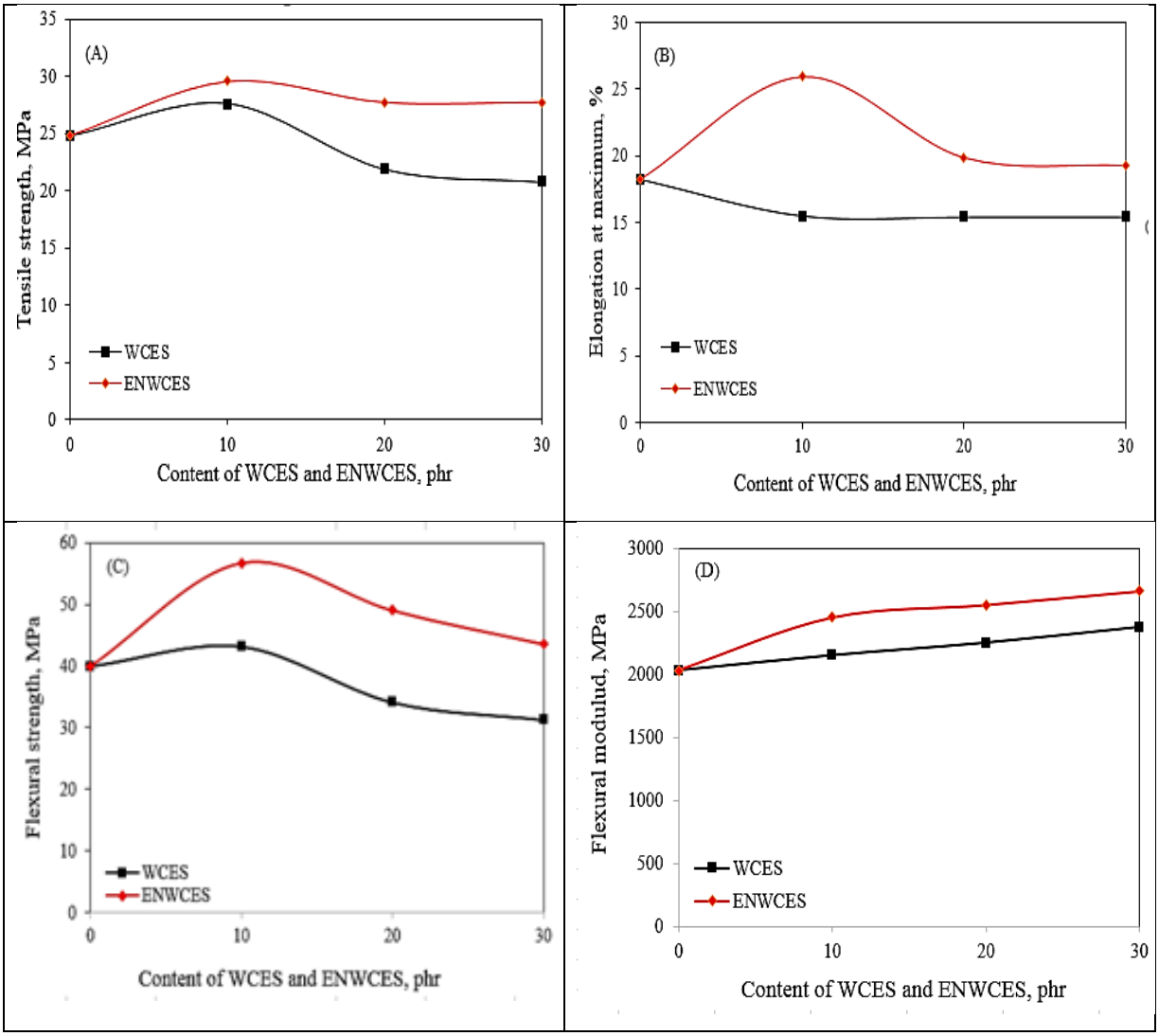

Figure 4: WPP/WCES and WPP/ENWCES composite mechanical characteristics

The flexural modulus of the WPP/ENWCES composites increments persistently with expanding the ENWCES loading up to 30 %. WCES improves the tensile and flexural strength of WPP composites when used in low content, according to the findings. At the point when WCES content increments the WCES will form agglomerates, as demonstrated in SEM micrograph (figure 2), which can depict as particles with higher dimensions, smaller surface contact area leads to decrement in the mechanical properties of the composites [45]. Figure 4 shows the WPP composites containing ENWCES (MOS5-7) have significantly higher mechanical properties than the composites containing WCES (MOS2-4).

This is mainly because the ENWCES enhances the interfacial interaction between filler and matrix. In the WPP/ENWCES composites, the chemical reaction of WCES particles reacts with NR-g-AAm, as shown in the FTIR spectra of WCES and ENWCES. This reaction decreases the hydrophilic characteristics of the WCES, resulting in increased compatibility between ENWCES and WPP matrix. In addition to the poor interfacial interaction between WCES aggregates and WPP matrix, as shown in the SEM micrograph (figure 2). These results illustrate the mechanical properties of WPP composites depend on surface contact area of the filler and on interfacial interaction between filler and WPP matrix [42].

Thermal aging is more predominant when the material is exposed to artificial heating rather than natural environmental heating. Figure 5 shows the impact of thermal aging on the mechanical properties of WPP composites. It shows that, the thermal aging has huge impact on tensile strength, elongation at maximum, and flexural strength of WPP composites. The tensile strength and flexural strength of the WPP/WCES and WPP/ENWCES composites increased as ageing time increased up to 4 days, then dropped as ageing time increased up to 7 days.

While the elongation at a maximum of WPP composites decreases continuously as the thermal aging time increases from 0 to 7 days. Since thermal aging causes crosslinking and crosslink cleavage in WPP composites. When aging was initiated, the rate of crosslink formation was more than that of crosslink cleavage. With increasing aging time, the rate of crosslink cleavage increased gradually. In addition to the organic matter of WCES and NR-g-AAm act as hydrogen peroxide scavengers and good antioxidants [46].

Dynamic mechanical properties

Dynamic mechanical properties were measured to examine the degree of filler-matrix or filler–filler interactions of WPP composites. Figure 5 G-H shows DMA curves of MOS1, MOS2, and MOS5 composites. The DMA parameters of neat MOS1, MOS2, and MOS5 composites are listed in Table 3.

Table 3: Dynamic mechanical analysis parameters of MOS1, MOS2, and MOS5 composites

Composite	tan δ_{max}	T_g /°C
MOS1	0.1007	-15
MOS2	0.0949	-17
MOS5	0.0815	+3

The storage modulus (E') and loss factor (tan δ) of the WPP composites are recorded as a function of temperature from -75 to 75 ˚C and shown in Figure 5 G-H. All the WPP composites show a glassy state that is followed by a rubbery state. Figure 5-G shows the decrease in the storage modulus of the WPP composites with the increase in temperature. This can be associated with the increase in the mobility of the polymer chains. The drop in the storage modulus of WPP composites with temperature during the transition from the glassy to the rubbery state occurs around 23 ºC for all composites. The MOS5 composite displays an increase in storage modulus in comparison to the MOS2 and MOS1 composites, respectively, under all temperature range. The storage modulus of the MOS5 composite increased by 66.38 and 124.53 % at -75 ºC compared to MOS2 and MOS1 composites respectively. Whereas, the storage modulus measured the recoverable strain energy in a deformed polymer, so it reflected the elastic modulus of polymer materials. The increase of the storage modulus of the MOS5 composite could be ascribed to a higher homogeneity in the composite resulted from enhancing the interfacial interaction between ENWCES and WPP matrix [47].

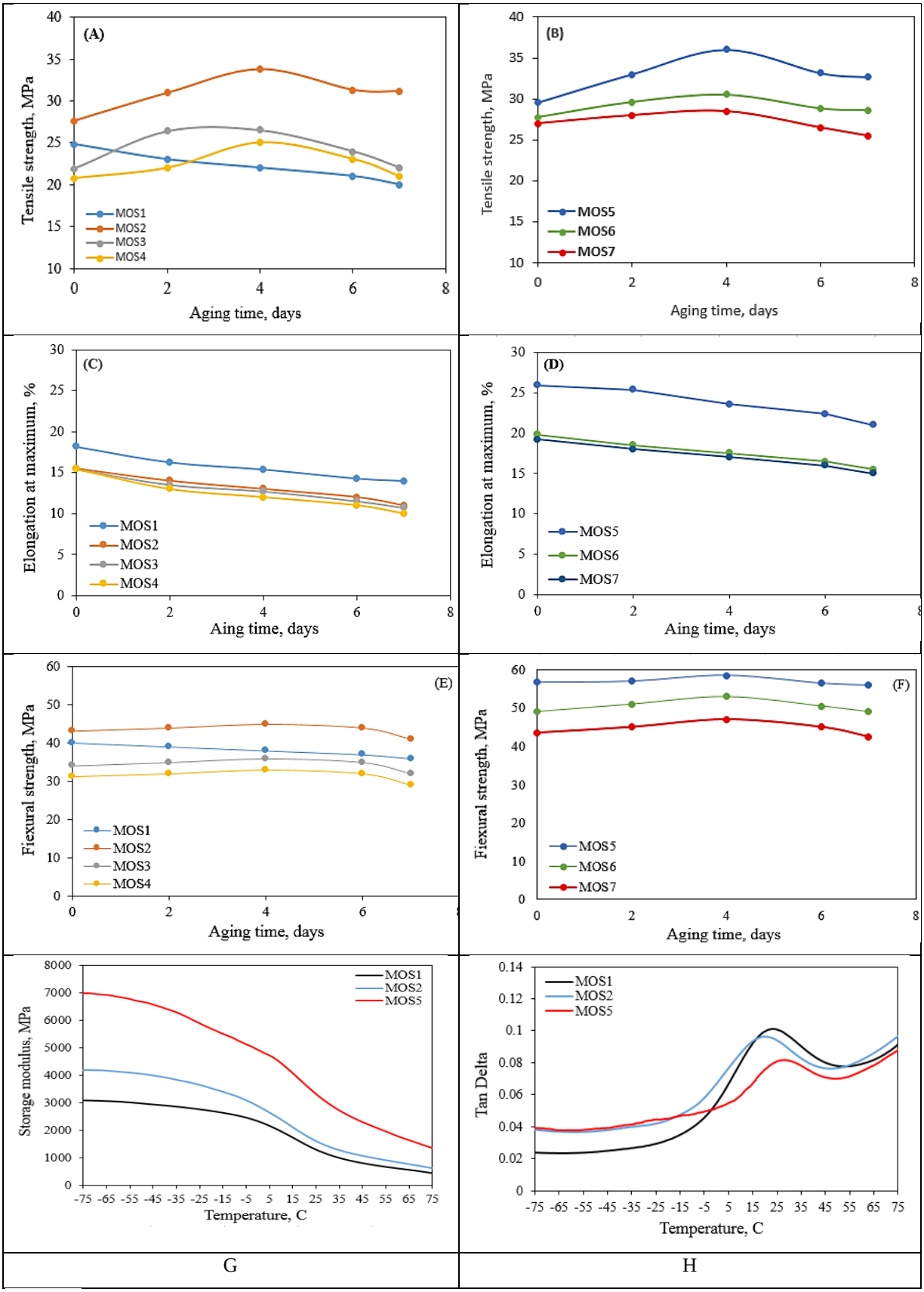

Figure 5: A-F) Relationship between the mechanical properties of WPP/WCES and WPP/ENWCES composites and aging time; G-H) Storage modulus (E^{l}), and loss factor (δ) curves as function of temperature for MOS1, MOS2, and MOS5 composites

Figure 5-H shows the presence of one characteristic transition that can be observed in the temperature range -75 to 75 ºC, and the glass transition temperature (T_g) at -15 ºC in the case of neat MOS1 composite. Tan δmax represents the height of the peak. Tan δmax is inversely related to the matrix-polymer filler interfacial adhesion. From Table 3, it can be noted that the T_g value of the MOS2 composite is less than that of the MOS1 composite because there is a weak interaction between WCES and WPP matrix, so there be a difficult transfer of load between the composite components [48]. With the addition of 10 phr of ENWCES in WPP matrix, the T_g value increased compared to that of the MOS1 composite as shown in Table 3. An increase of the T_g value and the lower tan δmax value were observed in the MOS5 composite. These changes may be due to the chemical reaction of WCES particles with NR-g-AAm that enhances the interfacial adhesion between the composite components and the dispersion of ENWCES in the WPP matrix.

Thermal Shrinkage

Figure 6-A illustrates the effect of heat at shrinkage of the specimens. The thermal shrinkage recorded the highest value at composite MOS1, then decrease by blending with 10, 20, and 30 phr of WCES to record 2.58, 1.77, and 1.69, for composites MOS2, MOS3, and MOS4, respectively. MOS5, MOS6 and MOS7 composites record 0.23, 0.11, and 0.04, respectively. It may be the encapsulation process enhances the compatibility between the composite's components.

Thermal Analysis

Figure 6-B illustrates the thermal degradation of the composites up to 700 ºC. The waste polypropylene (WPP) has one degradation stage that starts at 233 up to 458 ºC [2] with the highest weight loss percentage (99.0 %). At 700 ºC, the MOS1 composite records the lowest ash residue (1.0 %) due to the evaporated gaseous emitted from the decomposition of organic contents. This decomposition occurred during 225 ºC, it may return to the effect of oxygen on rate and mechanism of degradation, since the penetration of oxygen to some range less than the surface of PP. In the case of MOS2-4 composites, the degradation occurred between 200-420 ºC. The percentage of ash residue increase by increasing the weight of waste chicken eggshell, since MOS4 has the highest ash residue (16.6 %). It might get back to the low density of the produced gases like CO_2 and CO, which covered the specimen's surface with blocking of O_2 gas to respond with the combustible surface of the specimen.

In the case of MOS5-7 composites, they were more thermal stable than other composites up to 281 ºC, then start to degrade in between 281-455 ºC with high ash residue 10, 17, and 26 %, respectively. The composite MOS7 becomes more thermally stable and fire-resistant by consuming 30 min. to start in analysis and has the highest ash residue percentage (26 %) at the end of the test, which supports the composite to fight the ignition and extinguish it at a short 5 times. It was clear from tabulated data in Table 4, that modified WPP composites with microencapsulation technique have improved thermal and ignition characteristics of waste polypropylene. Whereas, new composites (MOS5-7) recorded the highest ash residue percentage during different temperatures up to 700 ºC

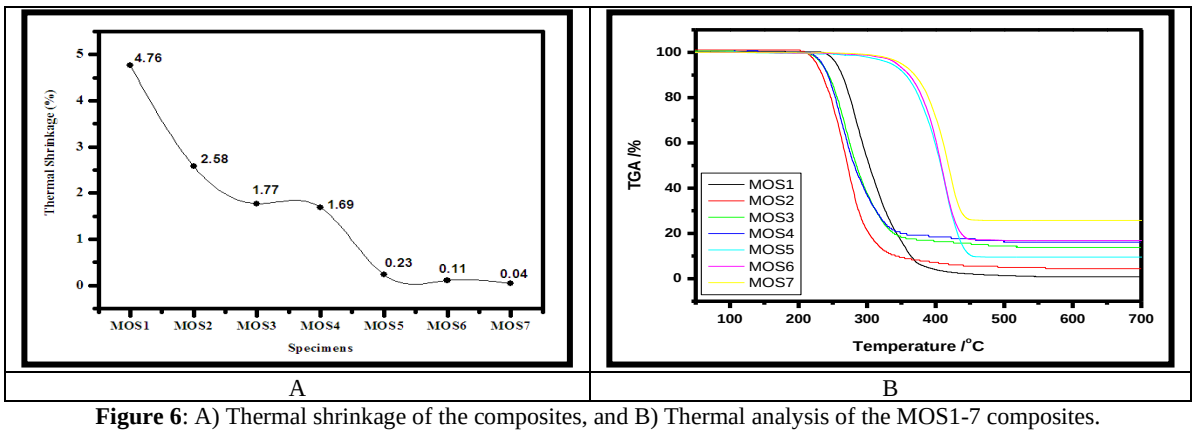

A B

Figure 6: A) Thermal shrinkage of the composites, and B) Thermal analysis of the MOS1-7 composites.

Table 4. Thermal analysis data from different analysis stages for untreated and treated composites at different temperatures.

Codes	0 ºC	300 ºC	400 ºC	500 ºC	600 ºC	700 ºC	T/ºC	T/ºC
	Weight %	Weight %	Weight %	Weight %	Weight %	Weight %	at 50 % of wt.	at 30 % of wt.
MOS1	100	53.2	03.6	01.6	01.0	01.0	302.7	327.1
MOS2	100	20.0	06.8	05.2	04.4	04.0	271.6	286.8
MOS3	100	36.4	16.4	14.2	14.0	13.9	284.4	310.6
MOS4	100	36.4	19.1	16.4	16.2	16.0	285.8	310.6
MOS5	100	97.2	58.7	09.1	09.5	09.0	406.9	422.1
MOS6	100	98.3	61.9	17.3	17.1	17.0	408.7	423.9
MOS7	100	98.9	72.4	26.8	26.4	26.0	417.9	436.7

Limiting Oxygen Index with Flame Chamber tests

The tests were performed with tabulated data in Table 5. The new composites MOS5-7 had the highest values compared to the others. The MOS1 composite was completely burned at 17.9 % of oxygen with melting, dripping, shrinking. This test goes with results from UL-94 since this specimen burning at a rate of 19.2 mm/min. The burning rate decreased by blending the WPP with different percentages of WCES (MOS2-4). It may return to surround the ignite specimen with non-compostable gases as CO and CO_2 which decrease the inter-chemical reaction with surround oxygen. These gases play an important role in decreasing the percentage of oxygen penetration to the outer surface of the specimen, so the inter-chemical reaction decreased and not burned completely with less smoking, shrinking, and dripping. By blending the WPP with a different weight percentage of WCES, the percentage of oxygen increased as percentage increase. The MOS4 recorded an oxygen index of 20.7% compared to composite MOS1 (17.9 %) with less smoking, shrinking, and dripping.

The ignition properties of the new composites (MOS5-7) were characterized by not being ignited at the normal conditions in presence of methane gas (UL-94) as a flame source and recorded the highest values of burning rate 26.6, 26.8, and 27.3 mm/min for MOS5, MOS6, and MOS7, respectively. Blending different wt.% from ENWCES rise the lowest % of oxygen from 20.7 % (MOS4) to 27.3 % in case of MOS7 with less shrinking, no dripping, and no burned completely.

Conclusion

Encapsulated WCES flame retardancy was successfully synthesized by using NR-g-AAm and WCES as a shell material. ENWCES was characterized by using FTIR, SEM, and X-Ray Diffraction techniques. ENWCES enhances the tensile strength, elongation at maximum, flexural strength, and flexural modulus of WPP/ENWCES composites compared to neat WPP and WPP/WCES composites. In case of 10 phr of ENWCES, enhancement of the tensile strength, elongation at maximum, and flexural strength of WPP composites were achieved thru 19.20 %, 42.70 %, and 41.85 %, respectively, compared to neat WPP composite. Thermal aging up to 4 days at 90ºC upgrades the tensile strength and flexural strength of the WPP/WCES and WPP/ENWCES composites. The storage modulus of the MOS5 composite was enhanced by 66.38 and 124.53 % at -75 ºC compared to MOS2 and MOS1 composites respectively. ENWCES composites improved the thermal and ignition characteristics of WPP composites since high stability with ash residue were recorded at new composites (MOS5-7). Human safety was achieved by resist ignition, no dripping, and no shrinkage up to 26.6 %.

Conflict of Interest

The authors declare that they have no known competing financial interests or personal relationships that could have appeared to influence the work reported in this paper.

Table 5: Oxygen index and burning tests of the MOS1-7 composites

Codes	LOI (%)	Notes	Burning Length (mm)	Burning Time (s)	Burning Rate (mm/min)	Notes
MOS1	17.9	Burned completely More smoking Shrinking and dripping	75.0	234.0	19.2	Burned completely More smoking Dripping
MOS2	19.3	Burned completely Less smoking Less shrinking and dripping	75.0	265.0	17.0	Burned completely Less smoking, shrinking, dripping
MOS3	20.2	Burned completely Less smoking Less shrinking and dripping	75.0	330.0	13.6	Burned completely Less smoking, shrinking, dripping
MOS4	20.7	Burned completely Less smoking Less shrinking and dripping	75.0	348.0	12.9	Burned completely Less smoking, shrinking, dripping
MOS5	26.6	Not burned completely Less shrinking and no dripping	------	------	------	No burning, shrinking, dripping
MOS6	26.8	Not burned completely Less shrinking and no dripping	------	------	------	No burning, shrinking, dripping
MOS7	27.3	Not burned completely Less shrinking and no dripping	------	------	------	No burning, shrinking, dripping

Acknowledgments

The authors thank Prof. Dr. Noha E. Khaled (President of National Institute of Standards), and Prof. Dr. Mohamed Badr El-Sabbah, Al-Azhar University, Faculty of Science, for their guidance and help to conduct this work.

References

[1] Moreno D.D.P., de Camargo R.V., dos Santos Luiz D., Branco L.T.P., Grillo C.C., Saron C., "Composites of recycled polypropylene from cotton swab waste with pyrolyzed rice husk" *J. Polym. Environ.*; 29, pp. 350-362;(2021).

[2] Younis A.A., El-Wakil A.A., "New composites from waste polypropylene/eggshell characterized by high flame retardant and mechanical properties" *Fiber. Polym*.; (2021), in press

[3] Girelli A.M., Scuto F.R., "Eggshell membrane as feedstock in enzyme immobilization" *J. Biotechnol.;* 325, pp. 241-249;(2021).

[4] Mohamed M.A., Mounir R., EL-Zayat M.M., Raslan H.A., "Physico-mechanical comparative study on gamma irradiated high density polyethylene/eggshell and commercial calcium carbonate composites" *Radiochim. Acta;* 109, pp. 485-492;(2021).

[5] Toro P., Quijada R., Yazdani-Pedram M., Arias J.L., "Eggshell, a new bio-filler for polypropylene composites" *Mater. Lett.;* 61, pp. 4347–4350;(2007).

[6] Bhagavatheswaran E.S., Das A., Rastin H., Saeidi H., Jafari S.H., H. Vahabi, Najaf F., Khonakdar H.A., Formela K., Jouyandeh M., Zarrintaj P., Saeb M.R., "The taste of waste: the edge of eggshell over calcium carbonate in acrylonitrile butadiene rubber" *J. Polym. Environ.;* 27, pp. 2478–2489;(2019).

[7] Dweiri R., "Processing and characterization of surface treated chicken eggshell and calcium carbonate particles filled high-density polyethylene composites" *Mater. Res*.; (2021), in press.

[8] Ghabeer T., Dweiri R., Al-Khateeb S., "Thermal and mechanical characterization of polypropylene/eggshell biocomposites" J. Reinf. Plast. Compos.*;* 32, pp. 402–409;(2013).

[9] Kumar R., Dhaliwal J.S., Kapur Shashikant G.S., "Mechanical properties of modified biofiller-polypropylene composites" *Polym. Compos.;* 35, pp. 708-714;(2014).

[10] Lin Z., Zhang Z., Mai K., "Preparation and properties of eggshell/ β-polypropylene bio-composites" *J. Appl. Polym. Sci.;* 125, pp. 61-66;(2012).

[11] Li J., Zhu X., Wang H., Lin P., Jia L., Li L., Chen Y., "Synthesis and properties of multifunctional microencapsulated phase change material for intelligent textiles" J. *Mater. Sci.;* 56, pp. 2176-2191;(2021).

[12] Balci-Torun F., Ozdemir F., "Encapsulation of strawberry flavour and physicochemical characterization of the encapsulated powders" *Powder Technol.;* 380, 602-612;(2021).

[13] Jaramillo A.F., Díaz-Gómez A., Ramirez J., Berrio M.E., Cornejo V., Rojas D., Melendrez M.F., "Eco-friendly fire-resistant coatings containing dihydrogen ammonium phosphate microcapsules and tannins" *Coatings*; 11, 280;(2021).

[14] Pithanthanakul U., Vatanyoopaisarn S., Thumthanaruk B., Puttanlek C., Uttapap D., Kietthanakorn B., Rungsardthong V., "Encapsulation of fragrances in zein nanoparticles and use as fabric softener for textile application" *Flavour Fragr. J.*; 36, 365-373;(2021).

[15] Jia D., Yang J., He J., Li X., Yang R., "Melamine-based polyol containing phosphonate and alkynyl groups and its application in rigid polyurethane foam" *J. Mater. Sci*.; 56, 870-885;(2021).

[16] Zhao W., Kundu C.K., Li Z., Li X., Zhang Z., "Flame retardant treatments for polypropylene: Strategies and recent advances" *Compos.-A: Appl. Sci. Manuf.*; 145, 106382;(2021).

[17] Wang Y.Z., Meng S., Wang F.C., Xiao T.Y., ZU L.W., Lan T.Y., "Synthesis of a novel flame retardant and study on its flame retardancy" *DEStech Trans. Eng. Technol. Res*.; (2017).

[18] Nithiyapathi C., Thirunavukkarasu K., Das A.D., Tamilvendan D., "Progression in fire retardant properties of polymer composites–A review, "In IOP Conference Series: Mater. Sci. Eng.; 1059, pp. 012058;(2021).

[19] Hajibeygi M., Mousavi M., Shabanian M., Habibnejad N., Vahabi H., "Design and preparation of new polypropylene/magnesium oxide micro particles composites reinforced with hydroxyapatite nanoparticles: A study of thermal stability, flame retardancy and mechanical properties" *Mater. Chem. Phys*.; 258, pp. 123917;(2021).

[20] Younis A.A., Mohamed S.A.A., El-Samahy M.A., Abdel Kader A.H., "Novel fire-retardant bagasse papers using talc / cyclodiphosphazane and nanocellulose as packaging materials" *Egypt. J. Pet*.; 30, pp. 25-32;(2021).

[21] Saeb M.R., Dakhel H.R., Ghaffari A,, "Mechanical properties and vulcanization characteristics of styrene-butadiene rubber (SBR) based compounds filled with eggshell powder as a bio-filler" AIP Conference Proceedings; 1042, pp. 312;(2008).

[22] Zhang H.Y., Liu K.K., "The synthesis of novel Schiff base antioxidants to promote anti-thermal aging properties of natural rubber" *Chem. Pap.;* 71, pp. 1481-1489;(2017).

[23] Zhang J., Guo J., Li T., Li X., "Chemical surface modification of calcium carbonate particles by maleic anhydride grafting polyethylene wax" *Int. J. Green Nanotechnol.: Phys. Chem*.; 1, 65–71;(2010).

[24] Abdel-Hakim A., El-Wakil A.A., El-Mogy S., Halim S., "Effect of fiber coating on the mechanical performance, water absorption and biodegradability of sisal fiber/natural rubber composite" *Polym*.; (2021), In press.

[25] Younis A.A., "Flame retardancy, mechanical properties and antibacterial activity for polyester fabric coated with a sol-gel coating and pomegranate rind" *Fiber. Polym*.; 20, 2594-2603;(2019).

[26] ASTM D638: Standard Test Method for Tensile Properties of Plastics (2014).

[27] ASTM D790: Standard Test Methods for Flexural Properties of Unreinforced and Reinforced Plastics and Electrical Insulating Materials (2017).

[28] Alsubari S., Zuhri M.Y.M., Sapuan S.M., Ishak M.R., Ilyas R.A., Asyraf M.R.M., "Potential of natural fiber reinforced polymer composites in sandwich structures: A review on its mechanical properties" *Polym*.; 13, 423;(2021).

[29] Jeong J., Lim Y., Park J., "Improving thermal stability and mechanical performance of polypropylene/polyurethane blend prepared by radiation-based techniques" *Eur. Polym. J.*; 94, 366-375;(2017).

[30] ISO 11358-1: Plastics - Thermogravimetry (TG) of Polymers - Part 1: General Principles (2014).

[31] ISO 4589: Determination of flammability by oxygen index. Geneva, Switzerland: ISO (2017).

[32] Younis A.A., "Optimization of mechanical, thermal, and ignition properties of polyester fabric using urea and phosphoric acid" *J. Ind. Text*.; 49, 791-808;(2020).

[33] ASTM D635: Standard test method for rate of burning and/or extent and time of burning of plastics in a horizontal position (2018).
[34] Younis A.A., El-Wakil A.A., "Improvement of mechanical and flame retardant properties of natural rubber by eco-friendly watermelon peel and crumb rubber" *Fiber. Polym*.; 22, pp. 1237–1246;(2021).
[35] Abdelkader R., Mohammed B., "Green synthesis of cationic polyacrylamide composite catalyzed by an ecologically catalyst clay called maghnite -H+ (Algerian MMT) under microwave irradiation" *Bull. Chem. React. Eng. Catal*.; 11, pp. 170-175;(2016).
[36] Punia S., Kumar M., Siroha A.K., Purewal S.S., "Rice bran oil: Emerging trends in extraction, health benefit, and its industrial application" *Rice Sci*.; 28, 217-232;(2021).
[37] Shah A.H., Zhang Y., Xu X., Dayo A., Li X., Wang S., Liu W., "Reinforcement of stearic acid treated egg shell particles in epoxy thermosets: Structural, thermal, and mechanical characterization" *Materials*; 11, 1872;(2018).
[38] Hubbe M.A., Rojas O.J., Lucia L.A., "Green Modification of Surface Characteristics of Cellulosic Materials at the Molecular or Nano Scale: A Review" BioRes.; 10, pp. 6095-6206; (2015).
[39] Taylor C.D., McClain J.B., Cole M., DeYoung J.P., Smoke C., "Polymer coatings containing drug powder of controlled morphology, U.S. Patent No. 10,898,353. Washington, DC: U.S. Patent and Trademark Office (2021).
[40] Lee S.H., Park S.Y., Chung K.H., Jang K.S., "Phlogopite-reinforced natural rubber (NR)/ethylene-propylene-diene monomer rubber (EPDM) composites with aminosilane compatibilizer" *Polym*.; 13, 2318;(2021).
[41] Cao Z., Daly M., Clémence L., Geever L.M., Major I., Higginbotham C.L., Devine D.M., "Chemical surface modification of calcium carbonate particles with stearic acid using different treating methods" *Appl. Surf. Sci*.; 378, 320-329;(2016).
[42] Poulose A.M., Anis A., Shaikh H., Alhamidi A., Siva Kumar N., Elnour A.Y., Al-Zahrani S.M., "Strontium aluminate-based long afterglow PP composites: Phosphorescence, thermal, and mechanical characteristics" *Polym*.; 13, 1373;(2021).
[43] Chen J., Jiang M., Su M., Han J., Li S., Wu Q., "Mineralization of calcium carbonate induced by egg substrate and an electric field" *Chem. Eng. Technol*.; 42, 1525-1532;(2019).
[44] Mahendra K.T., Shrikant P., Rakesh K.M., Snehasis J., "Characterization of thermal and physical properties of biofield treated acrylamide and 2-chloroacetamide" *Org. Chem. Curr. Res*.; 4, 1000143;(2015).
[45] Eiras D., Pessan L.A., "Mechanical properties of polypropylene/calcium carbonate nanocomposites" *Mater. Res*.; 12, 517-522;(2009).
[46] Xu N., Chen G., Liu H., "Antioxidative categorization of twenty amino acids based on experimental evaluation" *Molecules*; 22, 2066;(2017).
[47] Wang N., Mi L., Wu Y., Wang X., Fang Q., "Enhanced flame retardancy of natural rubber composite with addition of microencapsulated ammonium polyphosphate and MCM-41 fillers" *Fire Saf. J*.; 62, 281–288;(2013).
[48] de Brito E.B., Tienne L.G.P., Cordeiro S.B., Marques M.D.F.V., Monteiro S.N., "The influence of steam explosion treatment of green coffee cake on the thermal and mechanical properties of reinforced polypropylene matrix composites" *J. Mater. Res. Technol*.; 9, 4051–4060;(2020).